Evolution of geometric and electronic structure at the Bi/Ag(001) interface

T. Nakagawa,* Y. Saito, O. Ohgami, H. Okuyama, M. Nishijima, and T. Aruga†
Department of Chemistry, Graduate School of Science, Kyoto University, Kyoto 606-8502, Japan
(Received 8 June 2005; revised manuscript received 8 August 2005; published 5 October 2005)

Growth of Bi on the Ag(001) surface at 300 K has been studied. Low energy electron diffraction and scanning tunneling microscopy were used to reveal that the Bi/Ag(001) surface forms four distinct ordered structures upon deposition of Bi at 300 K, $c(2\times2)$, $c(4\times4)$, $p(4\times4)$-$p4g$, and $(\sqrt{5}\times\sqrt{5})R26.6°$ phases. A reversible phase transition from the $c(2\times2)$ structure to $c(n\times4)$, with $n=6-7$, upon cooling to ~240 K was observed. Another phase transition from the $c(4\times4)$ structure to $c(2\times2)$ upon heating was also observed. Angle-resolved photoelectron spectroscopy was used to study the evolution of the valence electronic structure. Several Bi derived surface states were observed along the high symmetry directions. A surface resonance band, split off from the Ag 5*sp* states, was observed along the edge of the Ag bulk band projected onto the (001) surface. This band is similar to that observed on In/Cu(001) and is considered to have a major contribution from the substrate states. Bi-6*p* derived bands, showing narrow bandwidth and periodicities coincident with the surface structure, were also observed.

DOI: 10.1103/PhysRevB.72.165405 PACS number(s): 73.20.At, 68.35.Bs, 71.45.Lr

I. INTRODUCTION

Heavier *p*-block metallic elements such as In, Tl, Sn, Pb, Sb, and Bi often exhibits crystalline structure with reduced symmetries, which suggests that the bonding in their solids has significant covalent character in addition to metallic one. This in turn suggests the strong electron-phonon coupling, as compared with those in, e.g., alkali metals and alkaline earth metals, indicating a larger possibility of peculiar phenomena driven by electron-phonon coupling such as density waves and superconductivity, in particular, in reduced dimensions. We actually have shown that Peierls-type charge-density-wave phase transitions take place in indium monolayers adsorbed on Cu(001).[1,2] We have been extending the study to monolayers of heavier *p*-block metallic elements other than indium. In this paper, we report on the detailed characterization of the atomic and electronic structure of bismuth monolayers on Ag(001).

Crystalline bismuth is a semimetal which has a low density of states at the Fermi level and a high electrical resistivity (130 $\mu\Omega$ cm at 300 K). The electronic configuration of Bi is $[Xe]4f^{14}5d^{10}6s^26p^3$, where the fully occupied 4*f* and 5*d* states can be considered as semicore states. The 6*s* subshell lies about 9 eV below 6*p* and hence is rather localized (inert pair effect). Thus the energy bands near the Fermi level is predominantly of 6*p* character.

The most stable structure of bismuth is the rhombohedral *A*7 structure with two atoms per unit cell. It consists of puckered sheets of bismuth atoms stacked in layers perpendicular to the trigonal [111] axis. Each bismuth atom has three nearest neighbors at a distance of 3.062 Å and the angle ∠Bi—Bi—Bi is 95.5°. The coordination number and the bond angle is consistent with the predominantly covalent bonding between p^3 hybridized Bi atoms. Because of such bonding character, the density of states at the Fermi level is very small, making Bi a semimetal. Recent angle resolved ultraviolet photoelectron spectroscopy (ARUPS) studies, however, have revealed that the surfaces of Bi are rather good metals, probably due to the breaking of bonds at the surfaces which reduces the covalency.[3]

The structure of ultrathin Bi films on metal surfaces are reported for a few metal surfaces.[4–6] According to these works, in the low-coverage films Bi atoms seem to have a tendency to form anisotropic structures such as a $(9\sqrt{2}\times\sqrt{2})R45°$ structure on Cu(001),[4] which might be in accordance with covalent bonding character of Bi. The structure of dense Bi films are characterized by quasihexagonal structures.

The Bi/Ag bulk phase diagram indicates only a very low intermiscibility and no intermetallic compound formation.[7] The surface free energy of Bi is 0.5 J/m^2, while that of Ag 1.2 J/m^2.[8] Although there is no available data for Bi—Ag interface energy, the large difference of the surface energies suggests that Bi films on Ag surfaces grow in a layer-by-layer fashion.[9]

In the present work we have studied the evolution of geometric and electronic structure upon the formation of ultrathin bismuth films on Ag(001). This paper is constructed as follows: In Sec. II, we describe the experimental procedures. In Sec. III, we show the experimental results for the geometric structure of Bi-covered Ag(001) surface investigated by Auger electron spectroscopy (AES), low-energy electron diffraction (LEED) and scanning-tunneling microscopy (STM); we reveal four ordered phases at room temperature and two reversible phase transitions induced by temperature change. We also present the ARUPS results which show the Fermi surface evolution with increasing Bi coverage and the electronic band structure of ordered phases. In Sec. IV, we discuss the nature of Bi—Bi bonding that governs the geometric and electronic structure based on the combined results obtained and the comparison with similar metal-on-metal systems. The detailed investigation regarding the phase transition will be published in a separate paper.

II. EXPERIMENT

Experiments were performed in two separate ultrahigh vacuum chambers, one for STM and the other for ARUPS.

The operating pressures were 5×10^{-11} Torr in the STM chamber and 3×10^{-10} Torr in the ARUPS chamber. Both chambers were equipped with LEED optics and ion sputtering facilities. The LEED optics were also used as retarding field analyzers to perform the AES measurement, in which the 1.2 keV primary electron energy was used. A variable-temperature STM (Oxford Instruments) with chemically etched polycrystalline tungsten tips was used to obtain images at sample temperatures from 70 to 300 K. All the STM images shown in this paper were taken in the constant-current (topographic) mode.

The ARUPS experiments were done with ARUPS10 (VG Microtech) and unpolarized He I radiation. The angular resolution was 1°. The energy resolution for energy distribution curves and Fermi surface (FS) mapping were set at 60 and 120 meV, respectively. The He I radiation used contained ~98% of He Iα (21.22 eV), ~1.5% of He Iβ (23.09 eV) and ~0.5% of He Iγ (23.74 eV). In most cases, the contribution of photoelectrons excited by He Iβ and He Iγ is negligible. However, when the bulk electronic states with high density of states are excited by these photons, it may give rise to photoelectron intensity comparable with that of the surface resonances excited by He Iα. Photoelectrons from Ag 4*d* excited by He Iβ and He Iγ are observed at binding energies, calibrated for He Iα, $E_B>1.5$ eV, and hence do not disturb the energy distribution curves close to the Fermi level. We determined work function from the overall spectral width of the photoemission spectra with the sample biased at −6.30 V. For Ag(001) surface we determined the work-function value as 4.40 eV, in agreement with the previous report.[10]

The Ag(001) samples were cleaned by repeated cycles of Ar ion sputtering at 700 eV and subsequent annealing at 850 K. The cleanness of the samples were checked by AES, observation of the sharp and uniform LEED patterns of the clean and Bi-covered surfaces, and STM. Additionally we checked that the Ag(001) surface state at $\bar{M}$ is clearly observed by ARUPS.[11]

Bismuth was evaporated from Knudsen-cell-type alumina crucibles which were carefully outgased before use. The operating pressure was maintained below 5×10^{-10} Torr. The Bi films were deposited at the substrate temperature of 300 K unless otherwise mentioned. The absolute coverage was estimated by directly counting Bi atoms using STM and by calibrating AES intensities by using low-temperature $(3\sqrt{2}\times\sqrt{2})R45°$ phase, whose structure was determined by dynamical LEED analysis,[12] as a reference. A monolayer (ML) is defined as the atomic density of 1.21×10^{19} atoms/m^2, corresponding to that of the Ag(001) surface. An evaporation rate of ~0.02 ML/min was used. With this procedure we can determine the coverage within ±0.05 ML. As shown below, the sticking coefficient of Bi onto Ag(001) at 300 K is constant up to $\theta_{Bi}=0.6$ ML. Above this coverage, the surface concentration of Bi in the surface layers accessible by AES remains constant even for prolonged deposition at 300 K.

III. RESULT

The growth and structure of Bi films on Ag(001) at 300 K was first characterized by studying AES and Bi derived LEED patterns as a function of Bi deposition time. The surface structure was then directly investigated by STM. The temperature dependent changes of the superstructures were studied by using AES and LEED, which showed phase transitions, including reversible and irreversible ones. Electronic structure of Bi on Ag(001) were investigated by ARUPS. These results are separately presented in the following sections.

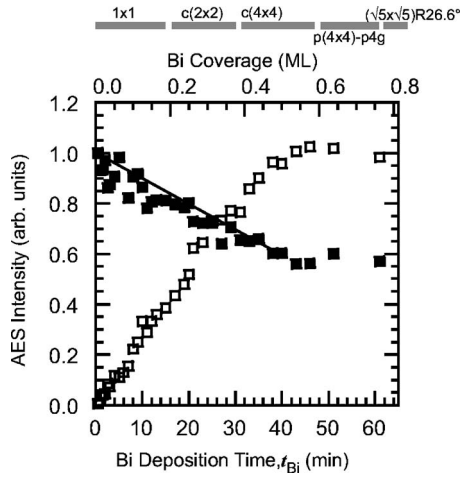

FIG. 1. AES uptake curves for Ag *MNN* at 353 eV (solid squares) and Bi *OVV* at 101 eV (open squares) measured at 300 K as a function of Bi deposition time. The solid line represents a fit to Ag Auger intensity based on the screening effect of Bi for the Ag Auger electrons. Also shown are Bi coverage and the corresponding LEED patterns (see Fig. 11 for the phase diagram).

A. AES measurement

Figure 1 shows the intensities of AES transitions for Ag *MNN*(353 eV) and Bi *OVV*(101 eV) as a function of Bi deposition time. As the Bi deposition time increases, the Ag AES intensity decreases linearly up to 45 min and then reaches a saturation value, 60% of that of the clean surface. On the other hand, the Bi AES intensity increases linearly up to 45 min and then reaches a saturation value. The additional deposition of Bi up to 180 min did not change the AES intensities of Ag and Bi. The almost constant intensity of the Ag AES intensity beyond 45 min coincides with the plateau of the Bi AES intensity, which indicates that the composition of Ag and Bi near the surface region accessible by AES remains constant above 45 min.

Several explanations may be possible for the constant AES intensity after 45 min: no sticking of further Bi on the Bi monolayer on Ag(001), the formation of thick Ag—Bi alloy with particular composition, or the penetration of further adsorbed Bi into deep bulk forming a solid solution. It is unlikely that the Bi atoms are not adsorbed on Bi-precovered Ag(001) surface at 300 K, since the vapor pressure of Bi is negligible ($<10^{-20}$ Torr) at 300 K. A TDS result for Bi/Cu(110) showed that multilayer Bi starts to desorb around 650 K and the desorption temperature of submonolayer Bi is even higher. The thick alloy formation at the surface may be possible. It is noted that even the surface

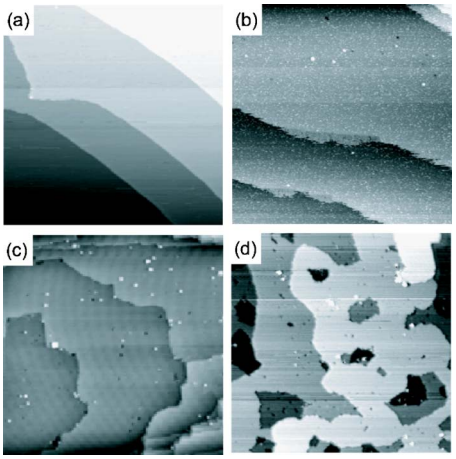

FIG. 2. Wide scan STM images for (a) clean Ag(001) surface (1000×1000 Å^2, $V_s=500$ meV, and $I_t=6'$ nA), (b) Ag(001) covered with 0.1 ML Bi (1500×1500 Å^2, $V_s=500$ meV, and $I_t=0.1$ nA), (c) 0.5 ML Bi (1500×1500 Å^2, $V_s=300$ meV, and $I_t=0.1$ nA), and (d) 0.75 ML Bi (1400×1400 Å^2, $V_s=100$ meV, and $I_t=1$ nA).

deposited with Bi for 180 min exhibits 1×1 LEED spots originating from the bulk Ag(001), which suggests that this alloy has a structure pseudomorphic to Ag(001). On the other hand, the $(\sqrt{5}\times\sqrt{5})R26.6°$ surface, which is observed for the surface deposited with a large amount of Bi, is unstable and is transformed back to $p(4\times4)$-$p4g$ several minutes after the Bi deposition is stopped. This indicates that there is a peculiar limit for the surface coverage of Bi and that thermal migration of Bi atoms takes place even at room temperature. The latter point may suggests that the constant AES intensity above 45 min is due to the rapid diffusion of excess Bi atoms dissolving into bulk Ag. The structure of the subsurface alloy, may it be intermetallic compound or solid solution, should be studied in future works.

B. STM results about morphological development

In Fig. 2, wide-scan STM images are presented which show morphological changes upon Bi adsorption. Figure 2(a) shows an image from the clean Ag(001)-(1×1) surface, which shows terraces with widths of several hundred Å, separated by monatomic steps. The STM image with $\theta_{Bi}\sim0.1$ ML shown in Fig. 2(b) shows terraces with many small protrusions on it. The protrusions are observed with an apparent height of ~0.5 Å and are elongated along the scan direction, indicating that they are Bi adatoms moving during the scan. Above $\theta_{Bi}=0.3$ ML ordered structures develop on the surface as shown later. At $\theta_{Bi}=0.5$ ML, the surface have still large terraces but the erosion or growth of the steps begins as shown in Fig. 3(c). At $\theta_{Bi}=0.75$ ML, hollows with monatomic step height appear as shown in Fig. 3(d). Note that the growth mode up to this Bi coverage is nearly two dimensional, and no preference of adsorption of Bi at step sites nor the formation of three-dimensional Bi islands on the surface is found.

C. Ordered phases

1. LEED

We found several ordered structures on Bi/Ag(001) as a function of the Bi coverage and the sample temperature. Here we present LEED results and atomically resolved STM images for the ordered phases. The LEED patterns obtained after the deposition of Bi at room temperature are shown in Fig. 3. With increasing Bi coverage, the (1×1) LEED pattern changes to a diffuse $c(2\times2)$ pattern around $\theta_{Bi}=0.3$ ML. Then the $c(2\times2)$ spots become intense and gradually change to a $c(4\times4)$ pattern. When the Bi coverage is slightly lower than the completion of the $c(4\times4)$ surface, streaks are present centering at 1/4th order spots along [11] direction, which is not removed even by cooling down to 110 K, indicating the existence of static disorder. The streaks disappear at the completion of the $c(4\times4)$ structure. A $p(4\times4)$-$p4g$ pattern appears at around 0.6 ML. For this pattern, $(n/2\ 0)$ and $(0\ n/2)$ spots are missing, indicating the presence of glide planes along the [110] and $[\bar{1}10]$ directions. Finally the LEED pattern shows a $(\sqrt{5}\times\sqrt{5})R26.6°$ pattern with weak $p(4\times4)$-$p4g$ background. Further prolonged Bi deposition does not change the LEED pattern. The $(\sqrt{5}\times\sqrt{5})R26.6°$ changes to $p(4\times4)$-$p4g$ several minutes after the deposition is stopped, which indicates that this structure is only possible with Bi atoms impinging from the gas phase.

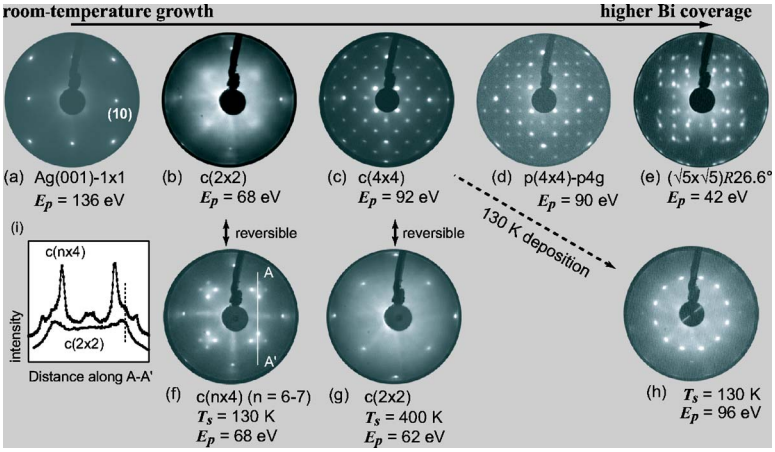

FIG. 3. (a)–(e) LEED patterns for the Bi/Ag(001) with the sample kept at 300 K with increasing Bi coverage. (f) and (g) LEED patterns induced by cooling and heating, respectively. (h) Hexagonal LEED patten ($T_s=130$ K) for a Bi multilayer (~3 ML) produced by Bi deposition onto the $c(4\times4)$ surface at 130 K. All patterns are taken at the normal incidence. (i) Line profile along the A-A′ line for the phase transition between (b) and (f).

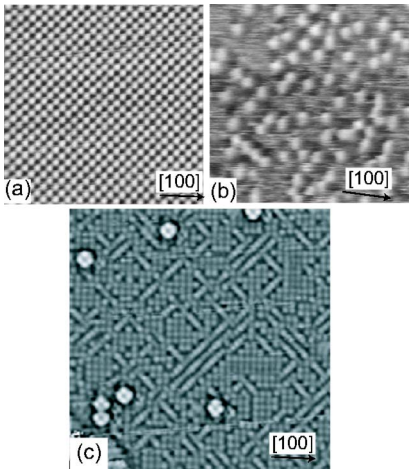

FIG. 4. Atomically resolved STM images for (a) clean Ag(001) surface (68×68 Å^2) at 300 K, (b) $\theta_{Bi}=0.1$ ML (90×90 Å^2) at 300 K, and (c) $\theta_{Bi}=0.35$ ML (160×160 Å^2) at 70 K.

The temperature change induces structural transitions. Cooling down the diffuse $c(2\times2)$ surface results in a LEED pattern shown in Fig. 3(f). Heating the $c(4\times4)$ surface results in a sharp $c(2\times2)$ pattern as shown in Fig. 3(g). These changes are reversible with respect to the temperature change.

Whereas hexagonal Bi growth is reported above 1 ML Bi coverage for various systems, for example, Bi/Cu(001),[4] a hexagonal LEED pattern is not obtained by Bi deposition on Ag(001) at 300 K. However, the hexagonal film is achieved when the $c(4\times4)$ surface is cooled down to 130 K, exposed to Bi at 130 K, and is subsequently annealed to 300 K. The resultant LEED pattern is shown in Fig. 3(h). The observed hexagonal pattern corresponds to a 2D hexagonal lattice constant of 4.5 Å, which is in good agreement with the corresponding value of the (111) surface of rhombohedral Bi, 4.53 Å. The diffraction spots from Ag(001) becomes very weak after deposition of ~3 ML of Bi, indicating epitaxial growth of a multilayer Bi(111) film on Ag(001).

2. $c(2\times2)$ and $c(n\times4)$ structures

An STM image taken at 300 K for the surface covered with 0.1 ML Bi is shown in Fig. 4(b), where protrusions with an apparent height of 0.5 Å are observed. The protrusions are not well ordered. The image is associated with considerable line noise along the scan direction, suggesting that the protrusions are moving on the surface. Around $\theta_{Bi}=0.3$ ML, we observed a weak and blurred $c(2\times2)$ LEED pattern at 300 K.

When the $c(2\times2)$ surface is cooled down, the LEED pattern gradually changes to one shown in Fig. 3(f) around $T=240$ K, with characteristic quadruplet spots around (1/2 1/2), which are indexed as (~0.4 0.5) and (~0.6 0.5), and weak spots at (~0.3 0), (0.5 0), and (~0.7 0). The transition is reversible with respect to the temperature change. We show in Fig. 3(i) the line profile for the two surfaces along a (1/2 1/2)-(1/2 −1/2) line. Whereas in the low temperature phase the (1/2 ~0.38) spot become intense, the intensity profile still show a small peak at (1/2 1/2). This shows that even at 110 K $c(2\times2)$ patches remain.

The STM image taken at 70 K at $\theta_{Bi}=0.35$ ML is shown in Fig. 4(c). The STM image contains three structural elements, $c(2\times2)$ domains, chain structures along [110], and a small numbers of bright tetramers. The chain structures are composed of linearly aligned protrusions with a spacing ~15% larger than that of Ag(001). The chains show intensity modulation with a periodicity of $6a-7a$, where a denotes the lattice constant of Ag(001), which seems to reflect the height difference of Bi atoms sitting on different lattice sites on Ag(001). The neighboring chains are separated by $2a$ and their intensity modulation is in antiphase. Thus the 2D unit cell for the chainlike structures are defined as $c(n\times4)$, where n varies about 6–7.

As seen in Fig. 4(c), there are patches of $c(n\times4)$ separated by $c(2\times2)$ domains. The interference between antiphase domains of $c(n\times4)$ should result in the apparent LEED pattern of $p(n/2\times2)$. Actually all the LEED spots observed for the low-temperature phase [Fig. 3(f)] is accounted for by $p(n/2\times2)$ and double diffraction from this superstructure and (1×1).

Worth to note is that on this low-temperature surface some isolated tetramers are seen. Interestingly, similar tetramers were also observed in a similar system, Ga/Ag(001) surface.[13] As shown below, at higher coverages the Bi tetramers are densely formed and are ordered in a $c(4\times4)$ symmetry.

3. $c(4\times4)$ surface

Figure 5(a) shows the STM image of the $c(4\times4)$ surface. The Bi tetramers, which were seen in Fig. 4(c) as isolated ones, are now ordered in a dense monolayer to form $c(4\times4)$. The density of the protrusions is 0.5 ML, which is in agreement with the Bi coverage. The nearest neighbor Bi—Bi distance is 3.0±0.1 Å, which is in moderate agreement with its metallic diameter. The STM observation suggests the fourfold ($p4mm$) symmetry of the $c(4\times4)$ surface.

For the $c(4\times4)$ surface with optimal coverage, STM shows that the whole surface is uniformly covered with the $c(4\times4)$ domain, in accordance with the highly contrasted LEED pattern as shown in Fig. 3(c). We note that antiphase domain boundaries were scarcely observed. This may indicate that the diffusion of Bi, possibly in a form of tetramers, occurs easily at 300 K to reduce the energy associated with the domain-wall formation.

Tetramer vacancies are often observed as shown in Fig. 5(a), but no one-, two- or three-atom vacancies are observed, indicating that the bonding within a tetramer is nearly saturated and the tetramer-tetramer interaction is relatively weak.

In Fig. 5(b), we show an STM image near the step on the $c(4\times4)$ surface. While the upper terrace is composed of $c(4\times4)$ alone, the near-step zone of the lower terrace shows $c(n\times4)$ and then $c(2\times2)$ structures. This indicates the step-induced shallowing of the adsorption well for Bi. The lattice strain and/or electrostatic potential may be responsible for this effect.

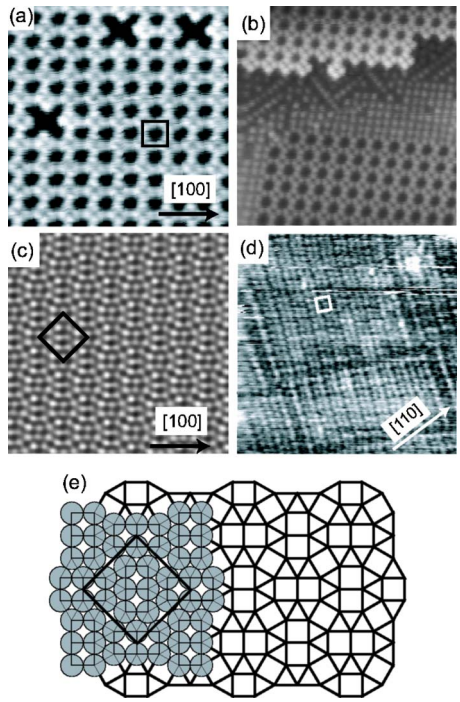

FIG. 5. (a)–(d) Atomically resolved STM images. Unit cells are marked by squares. (a) The $c(4\times4)$ surface (75×75 Å^2) with Bi coverage slightly less than 0.5 ML. (b) The structure near a step on the $c(4\times4)$ surface (75×75 Å^2). (c) The $p(4\times4)$-$p4g$ surface (80×80 Å^2). (d) The $(\sqrt{5}\times\sqrt{5})R26.6°$ surface (100×100 Å^2), prepared by Bi deposition at 200 K. (e) A model for the $p(4\times4)$-$p4g$ surface. The large square indicates a unit cell.

4. $p(4\times4)$-$p4g$ surface

Around 0.6 ML we observed a $p(4\times4)$-$p4g$ LEED pattern as shown in Fig. 3(d). The $(m/2\ 0)$ and $(0\ n/2)$ spots are missing, where n and m are odd integers. The missing spots indicate that this surface has glide planes along [110] and $[1\bar{1}0]$ directions. The STM image for this surface is shown in Fig. 5(c). The surface imaged was prepared by the deposition of ~1.0 ML Bi followed by subsequent annealing at 680 K for 5 min in order to get better-ordered surface. The STM image shows wide $p(4\times4)$-$p4g$ region, whose domains are limited only by the steps. The image clearly shows the existence of the glide planes in agreement with LEED. The density of the protrusions in this image is 0.75 ML. Assuming each protrusion as a single Bi atom, the coverage is in agreement with that for the most intense $p(4\times4)$-$p4g$ LEED pattern obtained. In Fig. 5(e), we show a schematic model for the $p(4\times4)$-$p4g$ structure. Interestingly, all Bi atoms are coordinated by five nearest-neighbor atoms.

5. $(\sqrt{5}\times\sqrt{5})R26.6°$ surface

Above 0.8 ML we observed additional spots in the $p(4\times4)$-$p4g$ LEED pattern as shown in Fig. 3(e), which we assigned to a $(\sqrt{5}\times\sqrt{5})R26.6°$ structure. While the $p(4\times4)$-$p4g$ spots in the LEED pattern remain, the spots from the $(\sqrt{5}\times\sqrt{5})R26.6°$ structure become more intense with increasing Bi coverage. When the $(\sqrt{5}\times\sqrt{5})R26.6°$ surface is left at room temperature for several minutes without deposition, the $(\sqrt{5}\times\sqrt{5})R26.6°$ spots become weak and finally vanish, whereas the $p(4\times4)$-$p4g$ spots become strong again. This phenomenon is repeatable and shows that the $(\sqrt{5}\times\sqrt{5})R26.6°$ surface is unstable at room temperature. As shown in the AES result, further deposition of Bi above 0.8 ML does not change the Ag and Bi AES intensities. As it took a few minutes to measure the AES intensity after the deposition, the AES result only reflect the Bi coverage of the stable structures. The excess Bi atoms added onto the $p(4\times4)$-$p4g$ surface cause the transformation of the $p(4\times4)$-$p4g$ structure to $(\sqrt{5}\times\sqrt{5})R26.6°$, but the penetration process competes with formation of the $(\sqrt{5}\times\sqrt{5})R26.6°$ structure.

We were not able to observe STM images of the $(\sqrt{5}\times\sqrt{5})R26.6°$ surface formed at room temperature due to its rapid conversion to the $p(4\times4)$-$p4g$ structure. Here we show a $(\sqrt{5}\times\sqrt{5})R26.6°$ surface which was obtained after the deposition of Bi at 200 K and transferred to the STM stage. The $(\sqrt{5}\times\sqrt{5})R26.6°$ structure obtained at $T_s=200$ K has a square-shaped unit cell. Within the unit cell, four protrusions are observed. This is similar to the Bi tetramer observed below $\theta_{Bi}=0.5$ ML, but in this case the tetramers are tilted by ~26° from the [110] direction and are ordered more densely than in the $c(4\times4)$ structure. Also seen are line dislocations running parallel to the sides of the unit cell. The density of the protrusions is 0.8 ML, in good agreement with the AES estimation.

D. Electronic structure

ARUPS measurement was carried out to study the evolution of the electronic structure at the Bi/Ag(001) interface. First, the electronic structure for the substrate, Ag, is briefly summarized. After the Bi-induced changes in the d-band region is shown, we concentrate on the Bi-induced changes in the Fermi surfaces and the band structure within 3 eV below the Fermi level, E_F, for the $c(4\times4)$ and $p(4\times4)$-$p4g$ surfaces. It is noted that for the $c(4\times4)$ and $p(4\times4)$-$p4g$ surfaces no projected band gap exists since the Ag bulk band is folded back by new translational symmetry of the surface. Thus all Bi-induced spectral features shown below are surface resonances. Figure 6(a) shows ARPES spectra for the $c(4\times4)$ surface at 120 and 300 K ($k_{\parallel}=1.79$ Å^{-1} at E_F along $\bar{\Gamma}\bar{M}$). As discussed below, the peaks at 0.7 and 2.2 eV are due to surface resonances induced by Bi adsorption, while the latter is overlapped with the Ag 4d peak excited by He $I\beta$ and $I\gamma$. The width of the surface resonance peak at 0.7 eV is rather broad (~0.3 eV) even at 120 K, which we ascribe to the interaction with the bulk Ag 5sp continuum. The peak becomes even more broad at 300 K, which is due to the phonon scattering. All photoemission data shown below were taken at 120 K unless otherwise noted.

1. Band structure of Ag(001)

The electronic structure of Ag consists of the broad 5sp bands and narrow 4d bands. Figure 6(b) shows ARUPS spec-

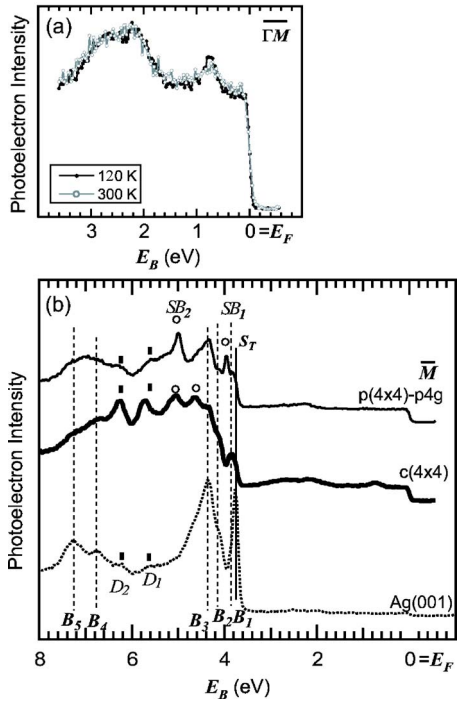

FIG. 6. (a) ARUPS spectra for $c(4\times4)$ surface taken at 120 and 300 K at $k_{\|}=1.79$ Å^{-1} at E_F along $\bar{\Gamma}\bar{M}$. (b) ARUPS spectra taken at 120 K for clean, $c(4\times4)$, and $p(4\times4)$-$p4g$ surfaces. The spectra were taken at $\theta_e=58°$ along [100], corresponding to $\bar{M}$ point ($k_{\|}=1.54$ Å^{-1}) at $E_B\sim4$ eV. Intensity of the Ag $4d$ surface state at 3.7 eV decreases with increasing Bi coverage, and at 0.5 ML the surface state is completely suppressed, whereas the bulk transitions, B_1-B_5, D_1 and D_2, are observed on Bi-covered surfaces.

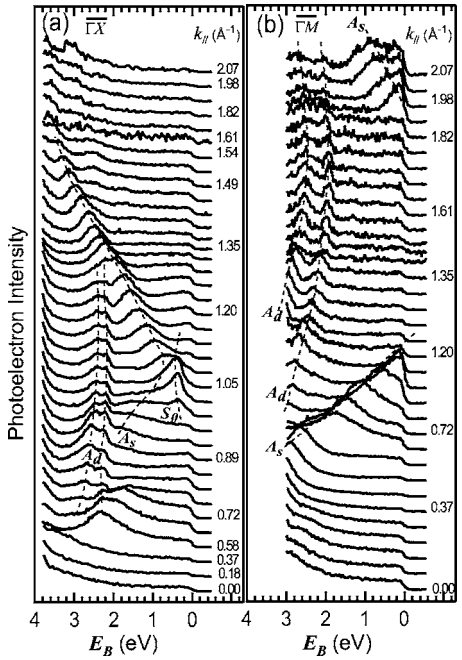

FIG. 7. ARUPS spectra for Ag(001)-1×1 surface along (a) $\bar{\Gamma}\bar{X}$ and (b) $\bar{\Gamma}\bar{M}$. The Ag $5sp$ band is denoted as A_s. The small peak around the $\bar{X}$ point with the binding energy of ~0.3 eV is due to a surface state. Note that the less dispersive peaks between 2 and 3 eV, denoted A_d, are due to photoemission from Ag $4d$ by He Iβ and Iγ radiations.

tra taken at the $\bar{M}$ point for the Ag(001)-(1×1), $c(4\times4)$-Bi, and $p(4\times4)$-$p4g$-Bi surfaces. The d bands of Ag are fully occupied and are located at binding energies $E_B>3.8$ eV. The spectrum for clean Ag(001) shows a very small Fermi edge and featureless region down to $E_B\sim3.7$ eV, where a sharp and intense peak, S_T, due to the Tamm surface state is observed.[11] The peaks due to the bulk states are observed at $E_B=3.9$, 4.2, 4.4, 6.8, and 7.3 eV in agreement with the previous result.[11] Peaks at $E_B=5.4(D_1)$ and 6.2 eV(D_2), are assigned to indirect density-of-states transitions.[14] Along the $\bar{\Gamma}\bar{M}$ direction, the bulk Ag $4d$ bands have local minima at 5.6 eV and 6.2 eV below E_F, leading to phonon-assisted, non-$k_{\|}$-conserving transitions. Very weak features at $E_B=2.0-3.0$ eV are due to the photoemission from the B_3 state excited by He $I\beta$ and $I\gamma$.

Deposition of 0.5 ML of Bi almost suppresses the S_T peak. Instead, the $4d$ bulk band, B_1, is clearly observed at $E_B=3.9$ eV, which is recognized at the tail of the S_T peak in the spectrum of the Ag(001)-1×1 surface. The complete depression of the Tamm state on the Bi/Ag(001) surface ensures the 2D growth of the Bi ultrathin film in agreement with the STM result.

The peaks at $E_B=4.6$ and 5.0 eV for the $c(4\times4)$ surface and 4.0 and 5.0 eV for the $p(4\times4)$-$p4g$ surface, indicated by circles in Fig. 6(b), do not have their origins in the Ag bulk band structure. The peaks (SB_1 and SB_2) on the $p(4\times4)$-$p4g$ surface shows relatively narrow widths compared with the Ag bulk bands, which indicates that these bands have surface origin.

The ARUPS spectra for clean Ag(001) for $E_B=0-4$ eV along [110] ($\bar{\Gamma}\bar{X}$) and [100] ($\bar{\Gamma}\bar{M}$) directions are shown in Fig. 7. The $\bar{\Gamma}\bar{X}$ and $\bar{\Gamma}\bar{M}$ distances are 1.087 and 1.537 Å^{-1}, respectively. The peak labeled as A_s corresponds to the bulk $5sp$ band. Note that the peaks, denoted A_d, localized between 2 and 3 eV in both directions are due to Ag $4d$ band excited by He $I\beta$ and $I\gamma$.

In Fig. 7(a), a band denoted as S_0 is observed along with Ag $5sp$ band near the $\bar{X}$ point.[15] The theoretical calculation showed that there exists a band gap at the $\bar{X}$ point, extending down to $E_B=0.5$ eV below E_F and the intrinsic surface state lies in the gap. As is seen in Fig. 7(a) the S_0 state shows a slight dispersion from $E_B=0.34$ eV at $k_{\|}=0.98$ Å^{-1}, which is close to the projected bulk band edge, to $E_B=0.36$ eV at $k_{\|}=1.08$ Å^{-1}, and loses its intensity beyond the $\bar{X}$ point. The S_0 state appears similar to the Shockley-type surface state observed on Cu(001) at the $\bar{X}$ point,[16,17] but shows a sharp peak only near the $\bar{X}$ point and becomes broad leaving $\bar{X}$. This indicates that the S_0 band does not cross the Fermi level, but hybridizes with the bulk state upon going away from $\bar{X}$.

2. Fermi surface mapping

The evolution of the 2D Fermi surface (FS) upon Bi deposition is summarized. Experimentally we measured photo-

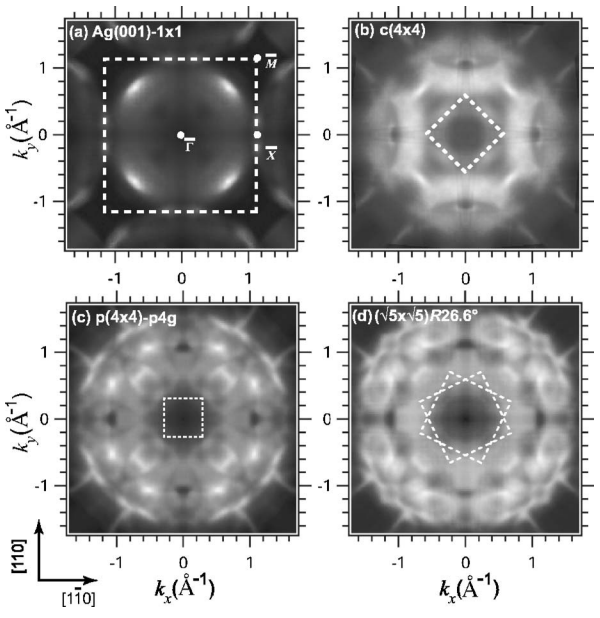

FIG. 8. 2D Fermi surface mapped with He I for (a) Ag(001)-1 $\times$1 surface, (b) $c(4\times4)$ surface, (c) $p(4\times4)$-$p4g$ surface, and (d) $(\sqrt{5}\times\sqrt{5})R26.6°$ surface. In each figure the first surface Brillouin zone boundaries are shown by dashed lines.

emission intensity over a 90° section by moving the analyzer with the energy window fixed at the Fermi level, and then constructed the FS maps (FSMs) presented in Fig. 8 by applying $p4$ symmetry operation. Figure 8(a) shows the intensity map for the Ag(001)-(1×1) surface. Circular feature is due to the bulk $5sp$ band. Along the $\bar{\Gamma}\bar{X}$ direction, no bands crossing E_F are observed, while along the $\bar{\Gamma}\bar{M}$ an intense feature is observed at 1.0 Å^{-1}, in agreement with the energy distribution curves [Fig. 7(b)].

Bi deposition changes FSM in two senses, appearance of Bi-derived Fermi surfaces and increase of the background. FSM for the $c(4\times4)$, $p(4\times4)$-$p4g$, and $(\sqrt{5}\times\sqrt{5})R26.6°$ surfaces in Fig. 8 exhibit these features. The circular feature from the Ag $5sp$ band becomes weak after Bi deposition. Several new features are observed due to the surface band structure derived upon Bi deposition. For $c(4\times4)$ surface, the most prominent ones are broad arches centering at $(k_x,k_y)=(\pm0.8,0),(0,\pm0.8)$. Folded-back, weaker ones are also seen centering at $(k_x,k_y)=(\pm1.2,0),(0,\pm1.2)$. Weak features are also observed at $k_F\sim0.45$ Å^{-1} along $\bar{\Gamma}\bar{M}$.

FSMs for the $p(4\times4)$-$p4g$ and $(\sqrt{5}\times\sqrt{5})R26.6°$ surfaces are more complicated. The one for the $(\sqrt{5}\times\sqrt{5})R26.6°$ surface is understood as superposition of contributions from two equivalent domains which are rotated by ±26.6° from the [110] direction. This agrees with its geometrical symmetry observed by LEED.

All three Bi/Ag(001) surfaces have considerably large Fermi surfaces, which is in contrast with bulk Bi. On the other hand, it has been shown that the surfaces of bulk Bi are highly metallic due to the bond breaking at surface.[3] Although the direct comparison is difficult for the Fermi surfaces of the Bi/Ag(001) interface, Bi surfaces and bulk Bi, the enhanced metallicity of the Bi/Ag(001) interface may be qualitatively understood by a mechanism similar to that for the Bi surfaces.

3. Band structure of the $c(4\times4)$ surface

We show the energy band structure for the $c(4\times4)$ and $p(4\times4)$-$p4g$ surfaces in this and the subsequent sections. In strong contrast with the previously studied In/Cu(001) system, where only one, nearly free-electron-like band was observed,[2] we observed many Bi-derived bands in the near-E_F energy region. This, of course, is due to the fact that a bismuth atom has three valence p electrons while indium has only one. (The $5s$ electrons of In and $6s$ of Bi lie in the deeper energy regions due to the inert-pair effect.) Nevertheless we found a similarity in the electronic structure of these two systems as shown below.

Figure 9(a) shows ARUPS spectra along the $\bar{\Gamma}\bar{X}$ direction. Figure 9(c) displays the corresponding gray scale representation of second derivative, $-d^2I/dE^2$. In the spectra between the $\bar{\Gamma}$ and $\bar{X}$ points, strong Ag $5sp$ emission (A_s) is observed. On the other hand, the Ag $5sp$ band in the second surface Brillouine zone (SBZ) is much suppressed.

Around the $\bar{X}$ point, we observed two parabolic bands with opposite dispersion: The S_0 band forms an electron pocket centered at the $\bar{X}$ point with its maximum binding energy of 0.4 eV, and becomes broader upon approaching E_F and crosses E_F at $k_F\sim1.0$ and 1.2 Å^{-1}, which is in agreement with the $k_F=0.8\pm0.2$ Å^{-1} and $k_F=1.2$ Å^{-1} in the FSM data [Fig. 8(b)]. On the other hand, S_1 has its minimum binding energy of 1.6 eV at the $\bar{X}$ point, and disperses downward. In the first SBZ, S_1 disperses roughly in parallel with the Ag $5sp$ band. Actually the S_1 band is located very close to the edge of the Ag bulk band projected onto the (1×1) surface, which is very similar to the surface resonance band observed on In/Cu(001).[2] On In/Cu(001), the surface resonance band constitutes a hole-pocket FS around $\bar{M}$,[18] but such a feature was not observed in the ARUPS spectra taken along $\bar{\Gamma}\bar{M}$ for Bi/Ag(001) as shown in Figs. 9(b) and 9(d). Also in contrast with the In/Cu(001) case, many other Bi-induced bands are observed on the Ag(001)-$c(4\times4)$-Bi surface. In addition to S_0, the S_2 band seems to constitute FS around $0.5\bar{\Gamma}\bar{X}$ and $1.5\bar{\Gamma}\bar{X}$. The S_2 band crosses E_F at $k_\parallel=0.58\pm0.07$ Å^{-1}. The band is also observed around $k_\parallel=0.17$ Å^{-1} and appears to form a hole pocket around $1.5\bar{\Gamma}\bar{X}$. High photoemission intensity at the Fermi edge at $k_\parallel\sim1.0$–1.5 Å^{-1}, may imply another Bi-induced band close to E_F. The bands denoted as S_4, S_5, and S_6 are symmetrically folded back about $k_x=0.5\bar{\Gamma}\bar{X}$ and $1.5\bar{\Gamma}\bar{X}$, which are zone centers of $c(4\times4)$ SBZ in a repeated zone scheme. The S_3 band is folded back about $k_x=0.75\bar{\Gamma}\bar{X}$ and $1.25\bar{\Gamma}\bar{X}$ corresponding to the SBZ boundaries.

Figure 9(b) shows ARUPS spectra along the $\bar{\Gamma}\bar{M}$ direction. An intense Ag $5sp$ band is observed, which rapidly disperses to E_F with increasing $k_\parallel$. Several Bi-induced bands are observed, but none of them appear to cross the Fermi level, which however is not consistent with the FSM data shown in Fig. 8(b) that indicates $k_F\sim0.4$ Å^{-1}. Extrapolation

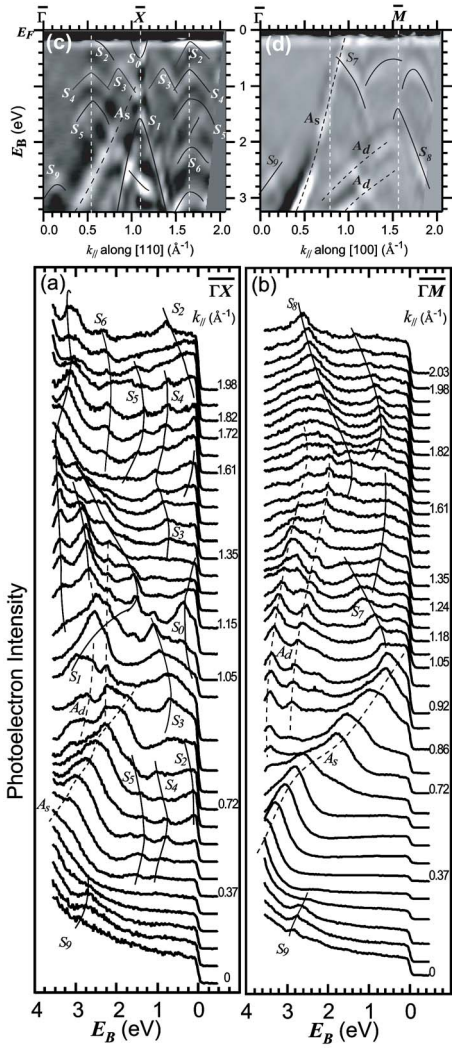

FIG. 9. ARUPS spectra and their gray scale representations for the $c(4\times4)$ surface between the binding energy of 0 and 3.5 eV. (a) ARUPS spectra along $\bar{\Gamma}\bar{X}$ direction. (b) ARUPS spectra along $\bar{\Gamma}\bar{M}$ direction. (c) Gray scale representation of $-d^2I/dE^2$ for the $\bar{\Gamma}\bar{X}$ direction. (d) The same as (c), but for $\bar{\Gamma}\bar{M}$ direction. The notations such as S_0,A_s for energy bands are explained in the text. In (a) and (b), the $k_{\|}$ values are indicated for E_B=0.

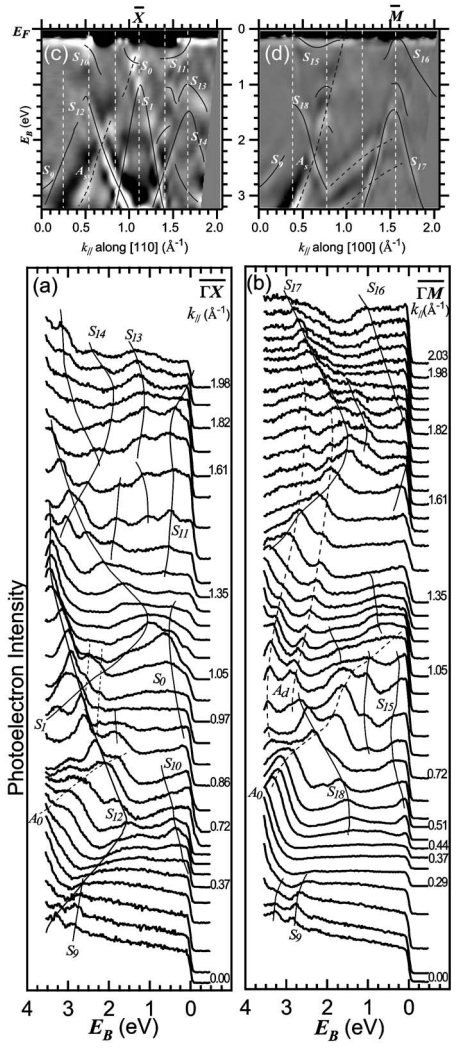

FIG. 10. ARUPS spectra and their gray-scale representations for the $p(4\times4)$-$p4g$ surface between the binding energy of 0 and 3.5 eV. (a) ARUPS spectra along $\bar{\Gamma}\bar{X}$ direction. (b) ARUPS spectra along $\bar{\Gamma}\bar{M}$ direction. (c) Gray scale representation of $-d^2I/dE^2$ for $\bar{\Gamma}\bar{X}$ direction. (d) The same as (c), but for $\bar{\Gamma}\bar{M}$ direction. In (a) and (b), the $k_{\|}$ values are indicated for E_B=0.

of the S_7 band seems to cross the Fermi level, which may explain FS at $k_F \sim 0.4$ Å^{-1}.

4. Band structure for the p(4×4)-p4g surface

Figure 10(a) shows ARUPS spectra for the $p(4\times4)$-$p4g$ surface along the $\bar{\Gamma}\bar{X}$ direction. The characteristic feature of the band structure observed in the $p(4\times4)$-$p4g$ surface is similar to that in the $c(4\times4)$ surface. The S_0 band is observed also on the $p(4\times4)$-$p4g$ surface, which has its maximum binding energy of 0.5 eV at $k_{\|}$=1.09 Å^{-1}, disperses upwards with decreasing $k_{\|}$. It crosses E_F at $k_{\|}$ =0.89±0.04 Å^{-1}. The Fermi vector associated with the S_0 band is observed in the FSM in Fig. 8(c). A circular-shape FS is observed around the $\bar{X}$ point in Fig. 8(c) implying that the S_0 band forms an electron-pocket FS. The S_1 band is also observed being centered at the $\bar{X}$ point with the binding energy of 1.2 eV. As compared to that on the $c(4\times4)$ surface, it is shifted to a lower binding energy by ~0.2 eV. The bands denoted as S_{10} and S_{11} appear to cross the Fermi level.

In Fig. 10(a), the band denoted as S_{12} is observed with the maximum binding energy of 3.3 eV at the $\bar{X}$ point. For the smaller emission angles, the S_{12} band disperses upward, has the minimum binding energy of 1.2 eV at $k_{\|} \sim 0.56$ Å^{-1}, which coincides with $0.5\bar{\Gamma}\bar{X}$, and disperses downward to reach $E_B \sim 3.2$ eV at the $\bar{\Gamma}$ point. For the larger momentum vectors beyond $\bar{X}$, the bands S_{13} and S_{14} are symmetrically folded back about $1.5\bar{\Gamma}\bar{X}$ with minimum binding energies of 1.2 and 1.9 eV, respectively. While the band connectivity is rather difficult to determine, these two bands may correspond to S_{12}.

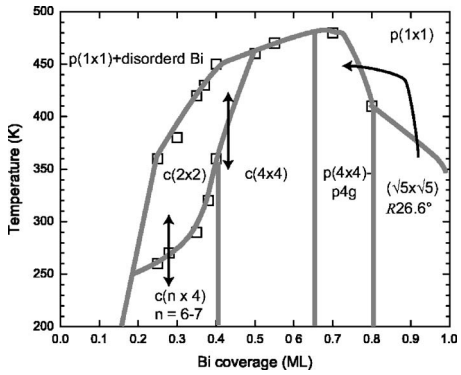

FIG. 11. Phase diagram for Ag(001)-Bi system prepared by deposition at 300 K. The squares indicates phase boundaries determined by LEED observation. The double-ended arrows indicate that the system undergoes reversible transition upon temperature change, whereas the single-ended one indicates an irreversible transition.

Figure 10(b) shows ARUPS spectra along the $\bar{\Gamma}\bar{M}$ direction for the $p(4\times4)$-$p4g$ surface. Along this direction, the Ag $5sp$ emission is observed at $E_B\sim3.5$ eV at $k_{\|}=0.34$ Å^{-1}, shifts upward and crosses E_F at $k_{\|}=1.0$ Å^{-1}, in agreement with FSM in Fig. 8(c).

A feature at $(k_x,k_y)\sim(0.4,0.4$ Å$^{-1})$ in FSM shown in Fig. 8(c) is understood as due to the S_{15} band, which appears to constitute a hole pocket around $\bar{\Gamma}$. Note that a hole pocket similar to this one is also observed on the $c(4\times4)$ surface. The S_{16} band also consititutes a small hole FS at $\bar{M}$, which can be seen in FSM in Fig. 8(c). The S_{17} band around $\bar{M}$ shows almost the same dispersion as that of the S_8 band on $c(4\times4)$.

IV. DISCUSSION

A. Structural evolution on Bi/Ag(001)

Figure 11 shows the phase diagram which summarizes the results of AES, LEED, and STM for the geometric structure observed as a function of Bi coverage and sample temperature. At low coverages (0.2–0.4 ML), LEED shows a diffuse $c(2\times2)$ pattern but it was difficult to take atomically resolved STM images, which suggests that the deposited Bi atoms move on the surface quickly at room temperature. On cooling down to 70 K, the lateral motion is suppressed and STM shows the chainlike $c(n\times4)(n=6-7)$ structure coexisting with $c(2\times2)$ patches for the surface covered with 0.35 ML Bi. Assuming that an individual protrusion corresponds to a Bi atom, we determine the local Bi coverages as 0.42–0.43 ML for the $c(n\times4)$ structure and 0.5 ML for the $c(2\times2)$ region. Further Bi deposition results in the $c(4\times4)$ structure, which appears to be composed of Bi tetramers, at the nomical coverage of 0.5 ML, the $p(4\times4)$-$p4g$ structure at 0.75 ML, and the $(\sqrt{5}\times\sqrt{5})R26.6°$ structure, which consists also of Bi tetramers, at 0.8 ML.

The results show that Bi and Ag do not form surface alloys at any coverages. This is in contrast with the similar systems, such as In/Cu(001) (Ref. 19) and Pb/Cu(111) (Ref. 20), in which heavier p-block metals are adsorbed on Cu surfaces. In the latter systems, surface alloys are formed at low coverages, indicating that the increased coordination by substrate atoms around an adsorbed atom results in the energy gain. This comparison may indicate that the adatom-adatom bonding is more important in the Bi/Ag(001) system. The formation of the highly anisotropic $c(n\times4)$ structure and tetramers in $c(4\times4)$ and $(\sqrt{5}\times\sqrt{5})R26.6°$ structures implies that the Bi—Bi bonding is not of purely metallic but has significant degree of covalent character. Similar tetramer structure was previously observed on Ga/Ag(001),[13] where Ga tetramers are stable at Ga coverages lower than 0.3 ML. On the other hand, as shown by ARPES, the Bi overlayer has metallic electronic structure, ruling out the completely covalent chemical-bonding picture. The bonding in this system should be located somewhere between the local covalent bonding and the delocalized metallic one. In other words, the electron-phonon coupling gives significant contribution in the metallic bonding in the Bi overlayer.

The Ag(001)-$c(4\times4)$-Bi surface also shows a phase transition, whose transition temperature depends on the Bi coverage. For low Bi coverages ($\theta_{\mathrm{Bi}}\sim0.4$ ML) the transition temperature is 340 K, and it rises to 450 K at the Bi coverage of ~0.5 ML. The phase diagram in Fig. 11 shows that this high-temperature $c(2\times2)$ phase is continuously connected with that observed at room temperature at lower coverages and is understood as a dynamically disordered phase where the Bi atoms are thermally mobile.

B. Bi—Ag interface electronic structure

Here we compare the electronic structure of Bi/Ag(001) with that of In/Cu(001). Indium atoms have the electronic configuration of $[\mathrm{Kr}]4d^{10}5s^25p^1$, while bismuth has $[\mathrm{Xe}]4f^{14}5d^{10}6s^26p^3$. The d and f shells are closed. The $5s$ and $6s$ subshells for In and Bi, respectively, are located rather deep in energy and do not have significant contribution to the valence band structure near E_F, which is often called an inert pair effect. Hence the observed valence band structure should be originated from the atomic p states and the substrate sp states. The main difference in atomic electronic structure between In and Bi is the number of electrons.

The In/Cu(001) surface has a surface resonance band, which runs along the edge of the projected bulk sp bands and shows a 2D nearly free-electron-like dispersion.[18,19] Along the $\bar{M}-\bar{X}-\bar{M}$ boundary, it shows a hybridization gap which divides the upper band, S_0, from the lower band, S_1. The evolution as a function of the In coverage was studied, which indicated that the bands are formed at the In—Cu interface.[19] The S_0 band is unoccupied at most of SBZ but constitutes an electron-pocket FS around $\bar{X}$, while the S_1 band constitutes a hole-pocket FS around $\bar{M}$.[18] The latter FS is square-shaped and has a close relevance to the phase transitions observed on this surface.[1,2,21]

On Bi/Ag(001), along $\bar{\Gamma}\bar{X}$ the S_0 and S_1 bands are observed on both the $c(4\times4)$ and $p(4\times4)$-$p4g$ surfaces. The

S_0 band has maximum binding energy of 0.4 eV on both surfaces at the $\bar{X}$ point, forming electron pockets. The S_1 band has minimum binding energies of 1.6 eV and 1.2 eV at the $\bar{X}$ point, respectively, on the $c(4\times4)$ and $p(4\times4)$-$p4g$ surfaces. The S_1 band is folded back at $\bar{X}$, which suggests that S_0 and S_1 are formed by the hybridization at the zone boundary. The overall dispersion of the S_0 and S_1 bands is very similar to those observed on In/Cu(001). Note that the minimum binding energy of the S_1 band is 1.3 eV for the $(9\sqrt{2}\times2\sqrt{2})R45°$ phase at $\theta_{\mathrm{In}}=0.5$ ML and 1.5 eV for the $c(4\times4)$ phase at $\theta_{\mathrm{In}}=0.63$ ML. The dispersion of the S_0 and S_1 bands strongly suggests that the contributions of the *sp* bands of the substrate, Ag or Cu, are dominant. This explains the fact that these bands are observed at almost the same energies on In/Cu(001) and Bi/Ag(001) even though the electronic configuration of Bi and In is much different. Note also that the energy and dispersion of the S_0 band on the $c(4\times4)$ and $p(4\times4)$-$p4g$ surfaces is similar to the A_0 surface-state band on the clean Ag(001) surface suggesting that the S_0 band has some contribution from A_0.

On the In/Cu(001), the S_1 band exhibits a dispersion along $\bar{\Gamma}\bar{M}$ with a slope almost the same as that along the $\bar{\Gamma}\bar{X}$ and crossed E_F at $\sim0.7\bar{\Gamma}\bar{M}$. This, however, is not the case on Bi/Ag(001). No such metallic band is observed on the $c(4\times4)$ or $p(4\times4)$-$p4g$ surfaces. Instead, the S_8 band on $c(4\times4)$ and the S_{17} band on $p(4\times4)$-$p4g$ exhibits a dispersion that can possibly be connected with the S_1 band. This suggests that the interface band on Bi/Ag(001) has a different slope according to the azimuthal direction, being deviated from the nearly free-electron band.

In contrast to the In/Cu(001) surface, many other bands are observed on Bi/Ag(001). The dispersion of these bands are not parallel with the parabolic one of the substrate *s* band and are considered as originating predominantly from the Bi 6*p* states. While some of the Bi-originating bands cross the Fermi level, many bands are weakly dispersed below the Fermi level, indicating a rather localized, covalent character of the Bi—Bi bonding within the Bi layer.

Strong electron-phonon coupling should, in principle, result in quasiparticle renormalization effect, which is then manifested by dispersion anomaly within the phonon energy scale from E_F in photoemission energy distribution curves.[22,23] It is difficult, however, to recognize such anomaly in the ARPES data shown in Figs. 9 and 10 due to the broad linewidth.

V. SUMMARY

We have investigated the geometric and electronic structure of Ag(001) covered with ultrathin Bi films. As to the atomic structure, we found six superstructures within submonolayer coverages for Bi deposition at room temperature. The atomic arrangements are observed using STM, in agreement with the symmetry observed by LEED. Above $\theta_{\mathrm{Bi}}=0.8$ ML, Bi does not show new phases and the AES intensity is constant, indicating the alloy formation or the penetration of Bi into bulk.

The electronic structure consists of nearly free-electron-like bands and narrower bands around E_F. We assigned the former band, S_0 and S_1, as derived from the Ag(001) 5*sp* band affected by the interaction with the Bi 6*sp* states. The latter bands are formed predominantly by the Bi 6*p* states. The electronic band structure suggests that the Bi overlayer has an intermediate character between metal and covalent solid.

*Present address: Institute for Molecular Science, Okazaki 444-8585, Japan.

†Email address: aruga@kuchem.kyoto-u.ac.jp

[1] T. Nakagawa, G. I. Boishin, H. Fujioka, H. W. Yeom, I. Matsuda, N. Takagi, M. Nishijima, and T. Aruga, Phys. Rev. Lett. **86**, 854 (2001).

[2] T. Nakagawa, H. Okuyama, M. Nishijima, T. Aruga, H. W. Yeom, E. Rotenberg, B. Kranzer, and S. D. Kevan, Phys. Rev. B **67**, 241401 (2003).

[3] M. Hengsberger, P. Segovia, M. Garnier, D. Purdie, and Y. Baer, Eur. Phys. J. B **17**, 603 (2000); S. Agergaard, Ch. Søndergaard, H. Li, M. B. Nielsen, S. V. Hffmann, and Ph. Hofmann, New J. Phys. **3**, 15.1 (2001); C. R. Ast and H. Höchst, Phys. Rev. Lett. **87**, 177602 (2001).

[4] F. Delamare and G. E. Rhead, Surf. Sci. **35**, 172 (1973).

[5] W. D. Clendening and C. T. Campbell, J. Chem. Phys. **90**, 2512 (1989).

[6] M. E. Jones, J. M. Heitzinger, R. J. Smith, and B. E. Koel, J. Vac. Sci. Technol. A **8**, 2512 (1990).

[7] M. Hansen, *Constitution of Binary Alloys* (McGraw-Hill, New York, 1958).

[8] V. K. Kumikov and Kh. B. Khokonov, J. Appl. Phys. **54**, 1346 (1983).

[9] H. Lüth, *Solid Surfaces, Interfaces, and Thin Films* (Springer, Berlin, 2001), p. 100.

[10] C. H. B. Mee, J. Phys. C **15**, 2305 (1982).

[11] A. Goldmann and E. Bartels, Surf. Sci. **122**, L629 (1983).

[12] T. Aruga, T. Nakagawa, Y. Saito, and H. Okuyama (unpublished).

[13] D. E. Bürgler, P. Hermann, S. Corbel, C. M. Schmidt, D. M. Schaller, P. Sautet, A. Baratoff, and H.-J. Güntherodt, Phys. Rev. B **57**, 10035 (1998).

[14] A. Goldmann, D. Westphal, and R. Courths, Phys. Rev. B **25**, 2000 (1982).

[15] L. Savio, L. Vattvone, M. Rocca, V. De Renzi, S. Gardonio, C. Mariana, V. del Pennino, G. Cipriani, A. Dal Corso, and S. Baroni, Surf. Sci. **486**, 65 (2001).

[16] S. D. Kevan, Phys. Rev. B **28**, 2268 (1983).

[17] A. Goldmann, V. Dose, and G. Borstel, Phys. Rev. B **32**, 1971 (1985).

[18] S. Hatta, H. Okuyama, M. Nishijima, and T. Aruga, Appl. Surf. Sci. **237**, 270 (2004).

[19] T. Nakagawa, S. Mitsushima, H. Okuyama, M. Nishijima, and T. Aruga, Phys. Rev. B **66**, 085402 (2002).

[20] M. L. Anderson, M. J. D'Amato, P. J. Feibelman, and B. S. Swartzentruber, Phys. Rev. Lett. **90**, 126102 (2003).
[21] S. Hatta, H. Okuyama, M. Nishijima, and T. Aruga, Phys. Rev. B **71**, 041401(R) (2005).
[22] M. Hengsberger D. Purdie, P. Segrovia, M. Garnier, and Y. Baer, Phys. Rev. Lett. **83**, 592 (1999).
[23] E. Rotenberg, J. Schäfer, and S. D. Kevan, Phys. Rev. Lett. **84**, 2925 (2000).